Journal of Engineering Research Innovation and Scientific Development 3 (2), (2025), 22-29 https://doi.org/10.61448/jerisd32255

Journal of Engineering Research Innovation and Scientific Development
journal homepage: www.jerisddelsu.com
Print ISSN 2971-6594 Online ISSN 2971-6608

Highly Efficient Adsorption of Co^{2+} from Wastewater on Alginate Immobilized Kaolin-Plantain Pseudo Stem-Snail shell Hydrochar: Isotherm modeling, Kinetics, Thermodynamic, and Mechanistic insight

Nneka Rosemary Agbale*[1], Lilian Ekiuwa Amoren[2], Judith Evawere Umukoro[3], Esther Nkechinyere Okoronkwo[4]

[1,3,4]*Department of Chemical Engineering, Faculty of Engineering, Delta State University, Abraka, Nigeria*

[2]*Department of Chemical Engineering, School of Engineering, Edo State Polytechnic, Usen, Nigeria*

Corresponding author: nragbale@gmail.com (Agbale N.R)

Article history: Received: 11-03-25, Revised: 12-05-25, Accepted: 25-05-25, Published: 30-05-25

Abstract

A major challenge in environmental remediation is the development of cost-effective processes that minimize the cost of energy and material while enabling the reuse of adsorbents for pollutant removal. Hydrochar (HC) is a promising substitute for biochar in environmental remediation, offering cost-effective, energy-efficient methods and enhanced regeneration through alginate immobilization. The adsorptive bahaviour of cobalt ions (Co^{2+}) from wastewater on HC and hydrochar encapsulated in alginate (AHC) under different conditions and the physiochemical properties of the adsorbents were examined in this study. AHC had the highest Co^{2+} adsorption efficiency (100%), followed by AL (94.56%) and HC (91.31%). The adsorption of Co^{2+} on HC and AHC was best fitted by the pseudo second order model, whereas the rate-determining steps were the Boyd diffusion and intraparticle diffusion models. The pseudo second order model provided the best fit for the adsorption of Co^{2+} on HC and AHC, while the intraparticle diffusion and the Boyd diffusion models were the rate determining steps. At all temperatures considered (25, 30 and 36 °C), the Freundlich isotherm model provided the best fit for the experimental data and the maximum adsorption capacities at these temperatures ranged between 81.66 to 98.04 mg/g. AHC demonstrated superior adsorption performance due to improved active site accessibility and surface interactions. Given its high adsorption efficiency, reusability, and environmental compatibility, alginate-based hydrochar composites (AHC) are recommended as a viable material for practical heavy metal remediation in wastewater treatment.

Keywords: Adsorption; Composite; Hydrochar; Alginate-encapsulated-hydrochar; Cobalt

1. Introduction

Heavy metal pollution represents a critical environmental issue that must be addressed to preserve the structure and functions of freshwater ecosystems (Zamora-Ledezmaet al., 2021). Globally, various industrial, domestic, and natural sources contribute to the release of heavy metals, disrupting ecosystem processes and threatening biodiversity. The pollution of freshwater systems impairs the ecological functions critical for maintaining environmental balance and adversely impacts the well-being of the flora and fauna (Chen X et al., 2019). The high mobility of cobalt, particularly in aquatic systems facilitates their bioaccumulation in organisms resulting in diseases like cardiomyopathy, dermatitis, neurological symptoms, hypothyroidism, and cancer in both aquatic species and humans (Ajibo et al., 2024). At elevated concentrations, these effects can be lethal, it becomes imperative therefore to reduce the pollutants to the minimal acceptable level before discharge or reuse for other purposes.

Various techniques, including adsorption, membrane processes coagulation/flocculation, precipitation, ion exchange, and biological methods, have been applied to mitigate Co^{2+} ion sorption from large wastewater volumes (Islam et al., 2018). Many of the techniques exhibit drawbacks like reduced removal efficiency, poor cost-effectiveness, dependency on stringent operational parameters, and excessive production of secondary sludge. Adsorption has proven to be a superior alternative for Co^{2+}removal, offering enhanced practicality, lower cost, and high efficacy, particularly at low ion concentrations (Awual et al., 2014). The application of low-cost adsorbents from naturally occurring materials, agricultural wastes and food wastes, as an alternative adsorbent for removing pollutants from wastewater has gained traction in recent years due to their operational feasibility, compatibility with engineering systems, cost advantages and environmental friendliness. As a result, significant effort has been directed toward identifying cost-efficient materials capable of selective metal ion detection and recovery.

Hydrochar (HC) as a cheap and efficient adsorbent, has proven to be highly effective in removing diverse types of pollutants. They are derived from the hydrothermal carbonization of biomass such as wood, bamboo, agricultural and forestry residues, kitchen waste, manure, and sludge (Nguyen et al., 2020). Although the pyrolysis of biomass to produce biochar (BC) offers numerous advantages, it involves high energy consumption, which leads to elevated operating costs. Moreover, the process may be less effective for materials like sludges and biomass such as plantain pseudostem (PSS) which has high affinity for atmospheric moisture absorption. .HC has been confirmed to exhibit a porous structure with chemically reactive surfaces and functionalized for various applications. Research has demonstrated that hydrochar, derived primarily from plant biomass, due to their low porosity and surface area, few adsorption sites and functional groups, exhibits lower adsorption efficiency compared to mineral-enriched HC and BC (Chen et al., 2019; Wang et al., 2021; Agbale et al., 2024). Studies have also revealed that both the mineral components and the carbonaceous fractions, particularly those with aromatic structures and oxygen-containing functional groups, play a significant role in the adsorption of heavy metals. The sorption efficiency is enhanced through the multiple means of interactions which include precipitation, electrostatic attraction, cation exchange and complexation (Xu et al., 2017). Also, mineral-based adsorbents with high content of calcium carbonate act as buffers in acidic water (Yoon et al., 2017). Alginate, which is derived from sea weed is a biodegradable polymer composed of mannuronic and guluronic acids. Its ability to bind multivalent cations makes it ideal for adsorbent entrapment in environmental remediation processes (de Araújo, et al., 2022). Alginate-encapsulated biochar and hydrochar beads are easily adaptable for fixed-bed column reactors. The characteristics of powdered BC and HC such as ease of recovery, mechanical strength surface area and functionalities, and hydraulic properties are enhanced upon immobilization in alginates (Wang et al., 2018).

Studies abound in which calcium carbonate biochar composite (Wang, et al., 2021; Gupta et al., 2021; Zhao, et al., 2022), and alginate immobilized biochar (Gürkan & İlyas, 2022; Gao et al., 2023; Kushwaha et al., 2024) are employed for the removal of heavy metals from wastewater. However, no work has been reported in literature for the adsorption of cobalt on alginate immobilized hydrochar synthesized from clay, natural calcium carbonate and biomass, which has a semblance to PMS In this work, a novel environmentally friendly high performing HC composite of high mineral content, and comprising of kaolin, plantain pseudo stem (PPS) and snail shell (SS) was synthesized and encapsulated into alginate (AHC) for the optimal removal of $Co^{2+}$from wastewater. The Adsorptive behavior of HC and AHC on the adsorption of Co^{2+} was studied.

2. Materials and Methods

2.1 Materials

PPS and SS are wastes obtained from a farm in Benin City, Nigeria (6.3350 °N , 5.6037 °E)., and kaolin was obtained from Freedom group of Companies, Benin City. Other chemicals such as $Co(NO_3)_2.H_2O$, $CaCl_2$ used (each of 99% percentage purity) and sodium alginate of 100 percent purity were all of analytical grade and obtained from Sigma-Aldrich Co. (Merck, Darmstadt, Germany).

2.2 Preparation of Kaolin-PPS-SS HC and HC encapsulated in Alginate

PPS and SS were washed in distilled water and dried in a drier for 48 hours. They were comminuted in a disk pulverizer to sizes of about 200 mesh. Kaolin, PPS and SS were mixed in the mass ratio of 5:10:5 prior to which the kaolin was stabilized in a sonicator for 1 hour and 30 minutes in 50 mL of ultra-pure water. The PPS and SS were added to the kaolin slurry in which another 50 mL water was added to make the mixture up to 100 mL and stirred for 1 hour at the rate of 300 rpm. The mixture was placed in a 200 mL autoclave and transferred to a muffle furnace (Laboratory Muffle Furnace SNOL 1,6,5.1/11 Ceramic, India) set

at a temperature of 180 °C., and residence time of 2 hours. The autoclave was removed after the set time, and cooled under running water. The HC was filtered in a Buchner funnel and dried in an oven at 95 °C for 24 hours.

The immobilization of the HC in alginate was done by mixing 2 % (w/v) of SA dissolved in distilled water and mechanically stirred at a temperature of 60 °C until it is completely homogenized. 4g of the dried HC was transferred into the SA solution and stirred with a magnetic stirrer at 240 rpm for 6 hours to achieve homogeneity. A syringe was used to suction the slurry, which was then dropped in tiny amounts into 200 mL of a 0.1 M $CaCl_2$ solution under vigorous stirring to form beads. During the addition of the homogeneous mixture to the $CaCl_2$ solution, continuous agitation of the composite-biochar-alginate and $CaCl_2$ solution was maintained using a magnetic stirrer to prevent the clustering of immature alginate beads The alginate beads formed were washed with distilled water, filtered off from the water, and dried in an oven at 40 °C for 6 hours and labelled AHC (Navarro etal.,m 2014). Pristine alginate beads were prepared by following the procedure for the hydrochar encapsulated alginate, however, HC was not incorporated into sodium alginate solution.

2.3 Batch Adsorption Experiments

A 100 ppm Co^{2+} standard solution was diluted to the desired concentrations using ultra-pure water. Adsorption experiments were conducted using a magnetic stirrer operating at a speed of 200 rpm. Batch experiments were carried out to investigate the effects of time, initial concentration, and temperature on the adsorption of Co^{2+} by HC and AHC. Kinetics studies were performed at a pH of 6, a temperature of 25 °C, and a sorbent dosage of 2 g/L, with residual Co^{2+} concentrations measured at 30-minute intervals up to 180 minutes. Initial Co^{2+} solution concentrations were prepared at 10 to 100 mg/L to study the effect of initial concentration on Co^{2+} adsorption by HC and AHC. Adsorption isotherm tests were conducted at temperatures of 25, 30, and 35°C, maintaining a constant pH of 6 and a sorbent dosage of 2 g/L. Residual Co^{2+} concentrations in the wastewater were measured using a spectrophotometer (model) under each adsorption condition. The adsorption capacity (qe or qt) and removal efficiency (%R) were enumerated from Equations 1 and 2 respectively.

$$q_e = \frac{(C_0 - C_e)v}{m} \quad (1)$$

$$\%R = \frac{C_0 - C_e}{C_0} \times 100 \quad (2)$$

where q_t (mg/g) and q_e (mg/g) are adsorption capacity at time t and at equilibrium respectively, V (mL) is the volume of solution, m (g) is the mass of the adsorbent. c_0 (mg/L) and c_e (mg/L) are the initial and equilibrium concentration of the solution, and c_t (mg/L) is the concentration at time t.

2.4 Characterization of Adsorbents

The functional groups of HC and AHC were analysed by Fourier transform infrared spectroscopy (FTIR) equipment (Perkin Elman Spectrum 3 FT-IR Spectrometer). The surface crystallinity was determined using the Bruker D2 Phaser. The Scanning Electron Microscope energy dispersive X-ray spectroscopy (SEM-EDS) Phenom Prox model, manufactured by phenom World was used to carry out the morphology analysis of HC and AHC.

2.5 Adsorption kinetics, Mass transfer, Isotherm models and Thermodynamics Models

The pseudo first order (PFO) and the pseudo second order (PSO) models were used to study the kinetics of the adsorption of Co2+ on HC and AHC. The linear forms of the Equations as shown in Equations 3 and 4 were used to evaluate these models.

$$\log(q_e - q_t) = \log q_e - \frac{k_1 t}{2{\cdot}303} \quad \text{(PFO)} \quad (3)$$

$$\frac{t}{q_t} = \frac{1}{k_2 q_e^2} + \frac{t}{q_e} \quad \text{(PSO)} \quad (4)$$

where, q_e and q_t (mg/g) are the amounts of substances removed from the aqueous phase by the biochar at equilibrium time and t, respectively; k_1 (min^{-1}) is the pseudo-first-order rate constant. The pseudo-first-order rate constant, k_1, was obtained from the slope of the linear plot of log (qe -q_t) vs t. k_2 (g/mg.min) is the pseudo-second-order rate constant. The second-order sorption rate constant k_2 (g/g.min) is determined from the intercept by plotting t/qt versus time t, whereas q_e is determined from the reciprocal of the slope of the straight line and k_2 equals quotient of the square of the slope and intercept (Biswas et al., 2018).

The Weber–Morris intraparticle diffusion (IPD) model and the Boyd et al models were used to evaluate the mass transfer mechanism in this adsorption process. The IPD model which is used to determine the mass transfer rate controlling step (Yakub et al.,2019) is given by Equation 5.

$$q_t = K_{IPD}\, t^{1/2} + C \quad (5)$$

where K_{IPD} is the intraparticle diffusion rate constant (mg/g $min^{1/2}$) and C (mg/g) is a is the interfacial film resistance or boundary layer effect. The Boyd et al (Boyd et al., 1947) mass transfer model was used to study the system to compare the particle diffusion with the film-diffusion

$$F_t = \frac{q_t}{q_e} = 1 - \frac{6}{\Pi^2} e^{(-\beta t)} \quad (6)$$

Where F_t is the fractional conversion, qt and q_e (mg.g^{-1}) are adsorption efficiency obtained at time t and equilibrium adsorption time, β is the mathematical function of F_t and t is the time in minutes. For values of F up to 0.05, Equation 6 reduces to

$$F_t = 1.08\sqrt{\beta t} \quad (7)$$

According to Reichenberg, (1953), if F_t lies between 0 and 0,85, then βt is expressed as:

$$\beta t = 2\pi - \frac{\pi^2 F_t}{3} - 2\pi\left(1 - \frac{\pi F_t}{3}\right)^{1/2} \quad (8)$$

And if F_t is between 085 and 1, βt becomes:

$$\beta t = -\ln\frac{\pi^2}{6}(1 - F_t) \quad (9)$$

The Boyd plot, representing a linear regression of βt against time (t) aids in distinguishing between particle diffusion and film diffusion-controlled adsorption. If the Bt versus time plot shows a linear regression fit passing through the origin, it indicates that the adsorption rate is controlled by particle diffusion. Conversely, if the fit does not pass through the origin, it suggests that film diffusion governs the adsorption rate (Wang and Guo, 2020).

The non-linear forms of the Langmuir and Freundlich isotherms were used to determine the best fitting isotherms for the adsorption processes. The Langmuir model represented in Equation 10 assumes that adsorption takes place on a uniform surface where all binding sites possess comparable energy and affinity for each adsorbate, indicating monolayer sorption behaviour (Touihri et al., 2021; Agbale et al., 2023)

$$q_e = \frac{q_m B_L C_e}{1 + B_L C_e} \quad (10)$$

The Freundlich isotherm(Singh, 2016) is presented in Equation 12 as

$$q_e = K_F C_e^{1/n} \quad (11)$$

where q_e is the equilibrium capacity (mg/g), qm is the maximum adsorption capacity (mg/g) B_L is the Langmuir constant (L/ mg), Ce is the equilibrium concentration (mg/L), K_F is the Freundlich constant (mg/g) $(L/mg)^{1/n}$ and n is the heterogeneity factor.

The change in enthalpy (ΔH°), entropy (ΔS°) and Gibb's free energy (ΔG°) were computed from Equations 12 and 13

$$\ln K_D = \frac{\Delta S^0}{R} - \frac{\Delta H^0}{RT} \quad (12)$$

$$\Delta G^0 = -RT \ln K_D \quad (13)$$

Where K_D is the equilibrium coefficient obtained from Langmuir isotherm at 25°C, 30 °C, and 35 °C

3.0 Results and Discussion

3.1 Preliminary Adsorption of Co^{2+} ions on the HC, AHC and pristine alginate beads

A comparative analysis of Co^{2+} ions adsorption by HC, AHC, and alginate is shown in Figure 1. The AHC had the greatest affinity towards the adsorption of Co^{2+} ions at a removal efficiency of 100 %. The pristine alginate beads closely followed this at 94.56. The tri-composite hydrochar adsorption performance was the lowest at 91.31%. Pristine alginate beads performed better probably due to the potential of alginate's rich surface functional groups (such as carboxyl and hydroxyl) to capture metallic or cationic ions through ion exchange between the crosslinking cations and target pollutants (like heavy metals or dyes) (Thakur et al.,2018). The low performance of the hydrochar, despite the high density of functional groups could be due to the agglomeration of the particles. This may have affected adsorption efficiency by reduction in surface area and mass transfer kinetics (Egbosiuba et al., 2024). The combination of alginate and hydrochar resulted in a synergistic effect which increased the adsorption efficiency of Co^{2+} on AHC. Although, the alginate performed better than HC, at the high temperature of 35 °C, it disintegrated due to its poor mechanical stability. Its use was discontinued for further studies.

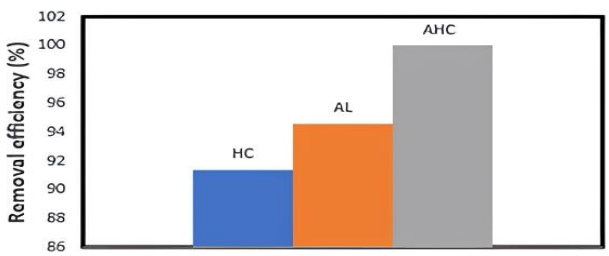

Figure 1: Comparison of the removal efficiency of Co^{2+} on Al, HC and AHC at a concentration of 50 mg/L, pH 5.6, an adsorbent dosage of 0.1g, time of 120 mins and a temperature of 27 °C

3.2 Effect of Contact time on the Adsorption of Co^{2+} on HC and AHC

Figure 2 (a and b) shows the effect of contact time on the adsorption of Co^{2+} onto HC and AHC respectively. The Co^{2+} adsorption rates of both adsorbents increased with time, as the adsorption equilibria were examined in the range of 30 to 180 mins. During the first 30 minutes of adsorbent-adsorbate interaction, the adsorption efficiency of Co^{2+} ions onto the adsorbents increased significantly. Thereafter, the process slowed down for both adsorbents. This happened as a result of a decline in active adsorption sites over time Wanet al., 2022). The high adsorption efficiency within the first 30 minutes is due to the high concentration of the pollutants which induce driving forces by difference in concentration gradient (Incan et al.,2024).

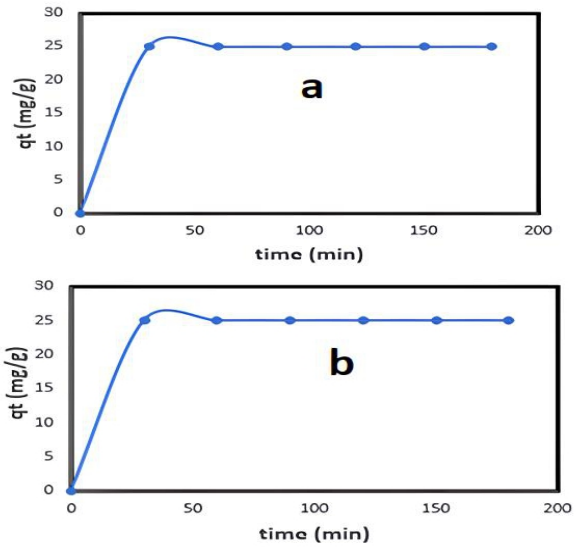

Figure 2: Effect of contact time on the adsorption of Co^{2+} onto (a) HC and (b) AHC. Conditions at PH 6, adsorbent dosage 0.1mg, volume of wastewater 50ml, temperature 27 °C.

3.3 Effect of Initial Concentration on the Adsorption of Co^{2+} ions on HC and AHC

The adsorptive behaviour of Co^{2+} ions on HC and AHC was studied by varying the initial concentrations between 10 and 120 mg/L, for each at 25 °C, 30 °C and 35 °C. To determine the dependence of the initial metal ions concentration in the aqueous phase and the metal sorption capacity of the adsorbent, the impact of initial metal concentration on biosorption is examined. Figure 3 illustrates how the adsorption efficiency of the metal ions depends on the initial concentration and rises with increasing initial concentration. For both adsorbents, the percentage of adsorbed Co^{2+} at all temperatures decreased as the initial concentration of the metal ions increased. The highest initial concentration of 120 mg/L had the lowest removal efficiency of which ranged between 50.3 and 56.9 of both adsorbents at the different temperatures. A high concentration of Co^{2+} ions caused the pores on the adsorbent surface to become more competitively dispersed in Co^{2+} ions (Rasheed et al., 2024) closing the pores and preventing Co^{2+} ions from moving into the absorbent's deep pores. Hence the initial concentration of metal ions supplies a driving force and also reduces the mass transfer resistance for allowing metal biosorption (González-Fernández et al., 2024) The removal efficiency at 25 °C reduced from 99.63 to 48.15% and from 99.9 to 50.9% on AHC and Al adsorbent respectively. The other results are 99.99 to 53% (AHC), 99.63 to 56.53 (AL) at 30 °C, and 99.9 to 54.98% (AHC) and 99.95 to 55.87% (AL) at 35 °C. There was a slight increase in removal efficiency and adsorption capacity as the temperature increased for each of the adsorbents. Similar trend was observed by Lim et al. (2022) in the adsorption of cobalt using alginate-immobilized biochar derived from buckwheat hull.

3.4 Kinetic and mass transfer studies

Kinetics models were used to investigate the type of adsorption, mechanism of adsorption and the rate controlling steps of the adsorption of Co^{2+} ions on HC and AHC at 25 °C (Yadav et al., 2022). The linearized forms of the two kinetic models, namely pseudo-first order, and pseudo-second order were used to determine the best fit kinetics. All the kinetic parameters (k_1, k_2, k_{id}, K_{FD}qe) and error function was evaluated using the coefficient of correlation R^2 are listed in Table 1. The best fitting kinetic model is evaluated based on the nearness of R^2 to 1.

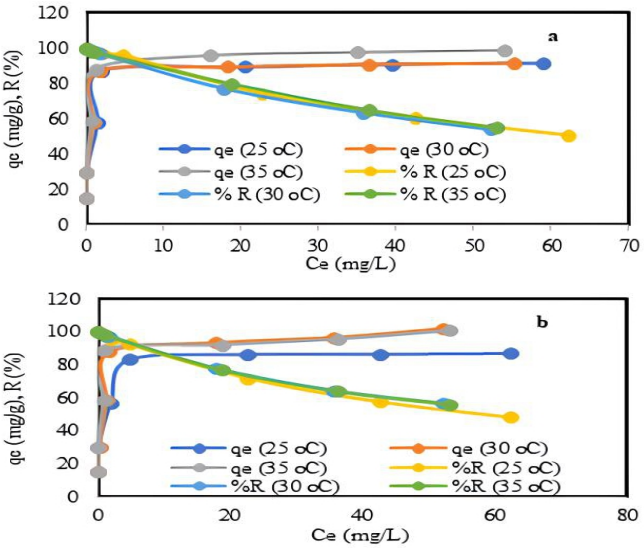

Figure 3: effect of initial concentration on adsorption. (a) on HC, (b) AHC at 180 minutes, 0.1g adsorbent dosage and pH of 6 at 25 °C, 30 °C and 35 °C.

Table 1 shows that the R^2 values of the pseudo-first-order model were much less than 1 and the values of the calculated equilibrium adsorption capacities ($q_{e(calc)}$) were much lower than the experimental equilibrium adsorption capacities ($q_{e(exp)}$) for the adsorption of Co^{2+} ions on HC and AHC. This implies that the model did not fit into the experimental data of the adsorption process. The values $q_{e(calc)}$ were calculated according to the pseudo-second-order model was equal to $q_{e,(exp),}$ and R^2 values were equal to 1.00 for the adsorption of Co^{2+} on both HC and AHC, indicating that the pseudo-second-order kinetic model fit well with the adsorption data. The perfect linear plot of t/q_t against t shown in Figure 4 further validates the fit provided by PSO to the experimental data. The PSO model is typically used to describe chemisorption processes rather than physisorption. Therefore, the exchange of electrons or valency between the Co^{2+} and the adsorbents during the adsorption process was not negligible (Wang et al. 2018). Similar results were obtained by Lim et al., (2022) and Rachdi et al., (2023). Lim and his colleagues studied the removal of Co^{2+} ions on biochar alginate composites the later studied the adsorptive removal of Cd on alginate encapsulated clay. The mass transfer rate controlling steps were evaluated by the Weber-Morris intra-particle diffusion and Boyd liquid film diffusion for the sorption of Co^{2+} ions onto HC and AHC beads were studied using Equations 5 to 9 and are shown in Figure 5. Generally, adsorption process mechanism is divided into three successive stages: the first stage is called the external diffusion of the particles, and the adsorbate diffuses from the solution to the surface of the adsorbent. The second stage is called pore diffusion, whereby the adsorbate continues to diffuse into the adsorbent pores in the adsorbent pores. The third stage is called the adsorption reaction stage, where the adsorbate is adsorbed on the surface within the pores of the adsorbent (Yakub et al., 2020). The intra-particle plot of the adsorption of Co^{2+} ions on AHC consists of only one step while that of HC has two steps. In the adsorption of Co^{2+} ions on AHC is there is only one rate-controlling step in the entire adsorption process. The rate-controlling step could be the boundary layer diffusion or the internal mass transfer. From the plot, the straight line of the IPD plot of AHC could be extended to approximately pass through the origin, this indicates that the external mass transfer is faster in relation to the boundary layer diffusion.

It was observed that plots of qt against $t^{0.5}$ for the adsorption of Co^{2+} ions on HC consist of two separate linear regions. It has been suggested that the first one can be attributed to external surface adsorption where the rate is high because of the large surface area and low competition between the Co^{2+} ions which are transported from the boundary film to the external surface of the adsorbent. Whereas the second portion of the plot indicates the intraparticle diffusion: transfer of Co^{2+} ions from the surface to the intraparticle active sites. It describes the slow adsorption stage of Co^{2+} onto HC caused by the low concentration gradient and finally produced the equilibrium condition (Zaghouane-Boudiaf et al., 2014).

The Boyd liquid film diffusion was used to further ascertain the rate-controlling step to evaluate the adsorption process. If the plot of –ln(1-qt/qe) against t does not pass through the origin and has a lesser error factor than the steps of the intraparticle diffusion plots, then the film diffusion controls the process (Boyd et al., 1947). From the values of $R^{2\,in}$ Table 1, and Figure 4,B, the criteria for film diffusion were satisfied. The plots of Al and AHC do not pass tthrough the origin and the value of $R^{2\,+}$ were high, 0.86 for HC, and 0.9412 for AHC. It can be inferred therfore, that, the rate-limiting steps of the adsorption involved both intraparticle and liquid film diffusion.

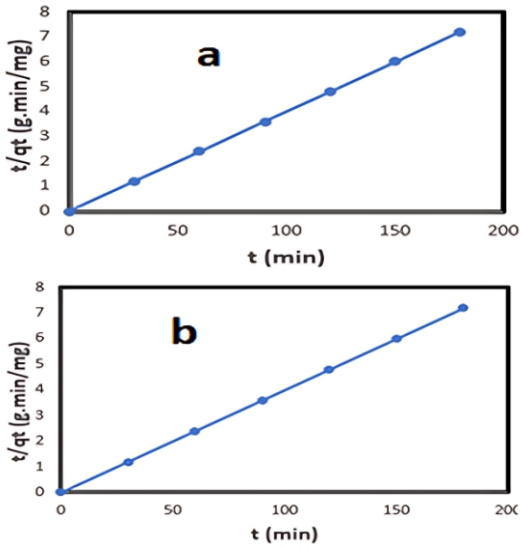

Figure 4: Pseudo second-order kinetics of the adsorption of C^{2+} on (a) HC and (b) AHC

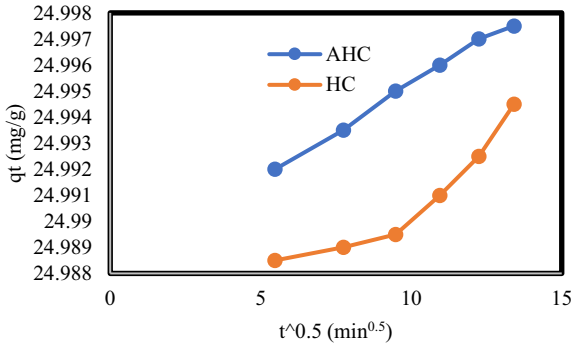

Figure 5a: IPD plot of HC and AHC

3.6 Equilibrium Studies

Finding a model that fits well enough for design work requires analyzing isotherm data using several isotherm models. The two-parameter Langmuir and Freundlich for the single component adsorption were used to evaluate the equilibrium adsorption experiments for Co^{2+} ions. Regression coefficient (R^2), Residual Sum of Squares (RSS) and Sum of Absolute Error (SAE) error values indicate the best-fitting isotherm, especially if the R^2 values of some of the isotherms are close (Nimbalkar and Bhat, 2021). A high incidence of $qe_{(calc)}$-Ce plots and $qe_{(exp)}$-C_e plots as shown in Figures 6 to 8 are required to further determine whether the isotherms are compatible with the adsorption data (Yu et al., 2018).

The isotherm studies for the adsorption of C^{o2+} from polluted water on HC and AH were conducted at 25, 30 and 35 °C. The parameters are represented in Table 2.

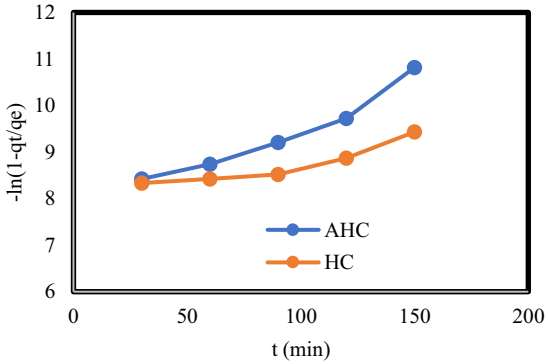

Figure 5b: Film diffusion plots of HC and AHC.

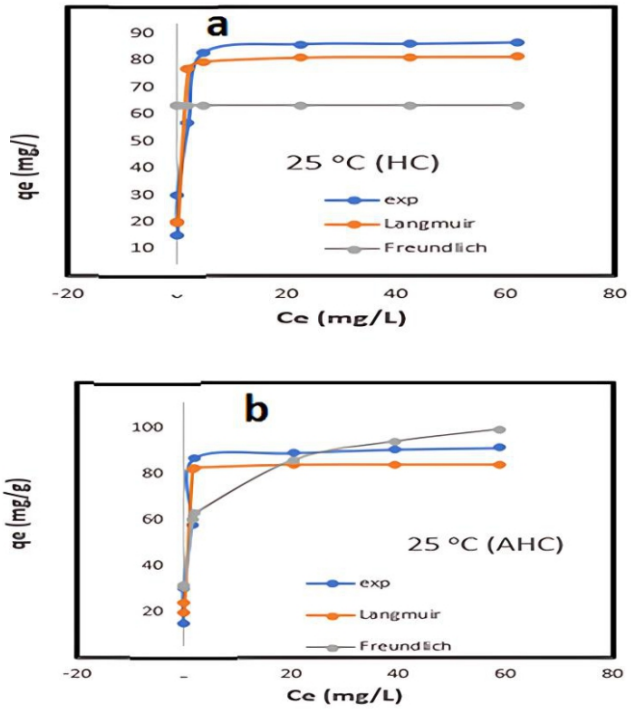

Figure 6: Non-linearized regression of Langmuir and Freundlich isotherm models parameters of the adsorption of Co^{2+} ions in wastewater at 25 °C on (a) HC and (b) on AHC

Table 1: Kinetic and Mass transfer Parameters

Model		Parameter	HC	AHC
Pseudo-first order		$q_{e(exp)}$ (mg/g)	25	25
		$q_{e(cacl)}$	1.04	1.06
		k_1 (min^{-1})	0.53	0.64
		R^2	0.5534	0.4230
Pseudo-second order		$q_{e(exp)}$ (mg/g)	25	25
		$q_{e(calc)}$	25	25
		k_2 (g/mg.min)	0.53	0.80
		R^2	1.00	1.00
Intra-particle diffusion	1st stage	k_{IPD1} (mg/(g·$h^{0.5}$)	0.002	0.0007
		C	24.99	24.99
		R^2	0.9752	0.9957
	2nd stage	K_{IPD2} (mg/g.$min^{0.5}$)	0.009	
		C	24.99	
		R^2	0.9943	
Film diffusion		K_{FD}	0.008	0.0183
		R^2	0.86	0.9412

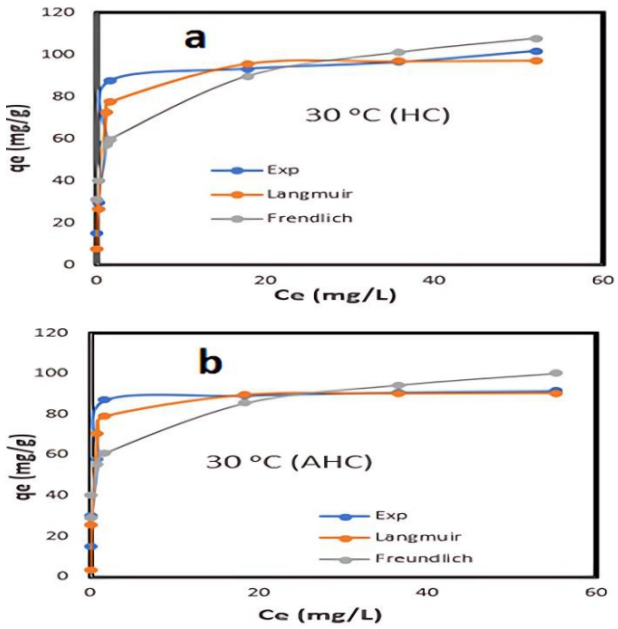

Figure 7: Non-linearized regression of Langmuir and Freundlich isotherm models parameters of the adsorption of Co^{2+} ions in wastewater at 30 °C on (a) HC and (b) on AHC

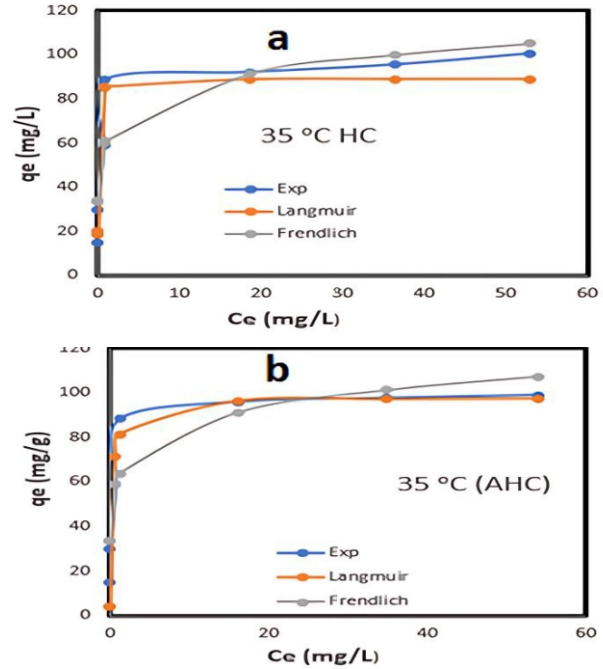

Figure 8: Non-linearized regression of Langmuir and Freundlich isotherm models parameters of the adsorption of Co^{2+} ions in wastewater at 35 °C on (a) AL and (b) on AHC

From the values of error functions, it is seen that the adsorption data of Co^{2+} ions on AL at 35 °C had a better correlation with the Langmuir isotherm than with the Freundlich isotherm. At other temperatures of 25, 30 and 35° for AHC, the Freundlich isotherm provided the best fit for the adsorption of Co^{2+} ions onto AL and AHC. The Freundlich isotherm assumes that the surface is multilayered, heterogeneous and have active sites with different energies (Zhao et al., 2021). The values of 1/n for all the mentioned adsorption processes were between 0 and less than 1. which implied that the adsorption process was favourable, and the adsorption is irreversible. The high values of K_F which was between 57.28 and 64.38 show that there are strong interactions between the adsorbate and the adsorption surface.

The R^2 values were also quite high, and the plots of all the Langmuir isotherms at all temperatures and in each adsorbent, being between 0.9776 and 0.9999, the Langmuir also provided a good fit for the adsorption data. The Langmuir isotherms depict adsorption occurring on a homogeneous surface with adsorbates dispersed in monolayers on the surfaces of the adsorbents. The maximum adsorption capacities were 81.66 and 98.04 mg/g

In the Langmuir isotherm, K_L is an important evaluation parameter related to the affinity of the binding sites. Since the range KL is greater than 0, the adsorption of Co^{2+} ions onto the AL and AHC is considered favourable.

3.6 Thermodynamics of adsorption

The temperature dependency of an adsorption process is a significant factor in the process mechanism. Changes in Gibbs free energy and entropy are crucial for predicting the spontaneity of an adsorption process. Whereas, the change in enthalpy is used to determine the direction of heat flow. Thermodynamic parameters also provide essential insights into the feasibility and efficiency of the process for practical applications. The values of ΔH^o and ΔG^o of the adsorption of Co^{2+} on HC and AHC presented in Table 3 show that the adsorption process is exothermic and spontaneous. High negative values of ΔH^o (HC: -175.85 and AHC: -60.65 kJ/mol) indicated an intense adsorbate-adsorbent interaction, implying that the process is chemisorption. This process, involving the formation of chemical bonds, is associated with significant energy shifts, generally in the range of -80 to -400 kJ/mol (Panic, Guzsvány et al., 2017). The positive change in entropy suggests that the disorder of the system increases during the adsorption process. This can occur if the adsorbed molecules displace solvent molecules or other species from the adsorbent's surface, leading to an increase in the overall randomness (Anastopoulos & Kyzas, 2016; Sharma et al., 2018)

Table 3: Thermodynamics parameters of the adsorption of Co^{2+} on HC and AHC at 25, 30 and 35 °C

Adsorbent	Temperature (°C)	ΔH^o (kJ/mol)	ΔS^o(J/mol)	ΔG^o (kJ/mol)
HC	25	-175.85	562.72	-343539
	30			-346353
	35			-349166
AHC	25	-60.65	212-04	-3359.8
	30			-3728.68
	35			-5506.61

3.7 Characterization of HC and AHC

The FTIR spectra of HC and AHC are shown in Figure 9 (a and b) respectively. Interestingly, reduced number of peaks appeared in AHC implying decreased functional groups were observed on the alginate immobilized hydrochar. This phenomenon could be due the encapsulation of the hydrochar in alginate masked the surface of the hydrochar (Younis et al., 2020). The O-H stretching peaks of HC and AHC occurred at 3657 and 3647 cm^{-1} respectively. Other peaks that are present include 1435 cm^{-1} which represents the C=C and-COO symmetric bonds of aromatics and carboxylates respectively (Shin et al., 2020). 1164 cm^{-1} corresponds to the C-O-C while the peaks situated at 958 and 861 cm^{-1} are Si-O vibrations which confirm the presence of kaolin. The presence of calcium carbonate was revealed by the peaks at 864 cm^{-1} belong to the vibrating groups (flexural vibration, asymmetric and symmetric tensile vibration) of the carbonate. The characteristic carbonate bands of aragonite were at 714 and at 864

Table 2: Langmuir and Freundlich Parameters for the adsorption of Co^{2+} ions on HC and AHC at three different Temperatures

Model	Parameter	HC			AHC		
		25 °C	30 °C	35 °C	25 °C	30 °C	35 °C
Langmuir	qm mg/g)	89.12	98.04	81.66	97.72	90.93	84.25
	K_L	26.66	2.30	8.55	4.38	3.87	30.26
	R^2	0.9853	0.9972	0.9998	0.9776	0.9916	0.9999
	RSS	15.31	54.69	6.71	109.2	158.81	0.23
	SAE	3.91	7.39	2.58	10.24	12.60	0.48
Freundlich	K_F ((mg/g)·(L/mg)$^{1/n}$)	64.38	54.91	61.83	62.66	56.38	57.28
	1/n	0.00	0.17	0.13	0.13	0.14	0.14
	R^2	1.00	0.9996	0.997	0.9996	0.9996	0.9996
	RSS	1.6 x10^{-13}	24.53	18.43	22.77	22.45	16.74
	SAE	4.2 x10^{-7}	4.95	4.28	4.77	4.73	4.09

cm^{-1} revealed the availability of aragonite form of calcium 3carbonate in the shell, The peaks around 491 and 542 cm^{-1} indicates the presence of Al-O, Al-O-Si, and Si-O (Reddy and Lee, 2014; Rafiq, et al., 2017).The peaks at 861 and 1154 cm^{-1} in AHC spectra suggests the presence of mannuronic and uronic acid derived from the alginates.

The XRD pattern of HC and AHC are depicted in Figure 7 (c and d) respectively. The peaks around 2θ = 12.78, 23-31, 33.43 and 36.65° represent kaolinite, quartz, aragoniteand amorphouscarbon respectively(Dewi et al., 2018; Rallet et al., 2022). The values at 2θ = 23.0 and 43.30° represent the presence of graphite while the peaks around 27.19 and 43.30°are attributed to sylvite, due to the presence of inorganics such as K, Cl, and Ca. Quartz refers to the presence of silica, which provides additional mechanical strength, improves thermal stability, enhances adsorptive properties, and potentially aids in catalytic or environmental applications. The presence of quartz in biochar enhances its functionality (Oyewo et al., 2023). The humped peaks at 44 ° are due to the presence of amorphous carbon. peaks which ranged from 23.02-23.06, 29.37-29-39, 35.97-35.9° and 43.15 up to 80. 55 is calcite. Calcite is thermodynamically stable and of great significance to the remediation of the environment.

The SEM images depicted in Figure 9(e and d) show that the AHC has more openings than the HC. The surface of HC is rougher and the particles were agglomerated in clusters. The highly microporous structure of AHC may be indicative to an increased surface area which provided more active sites for the adsorption of cobalt, thus its higher adsorption efficiency.

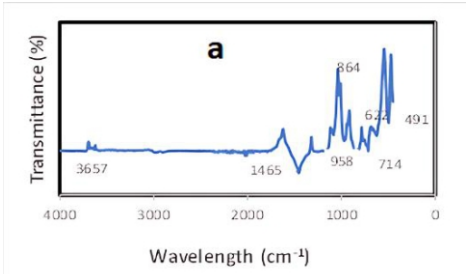

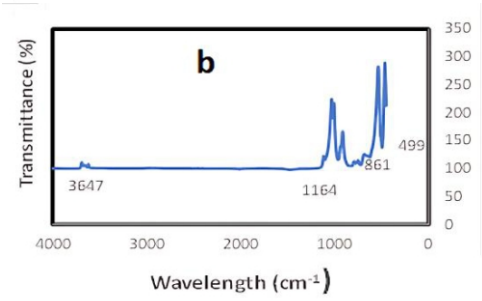

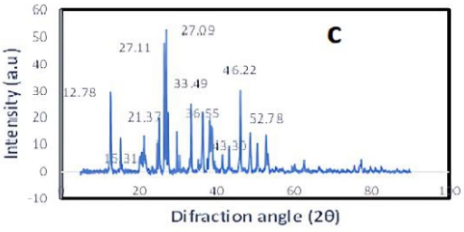

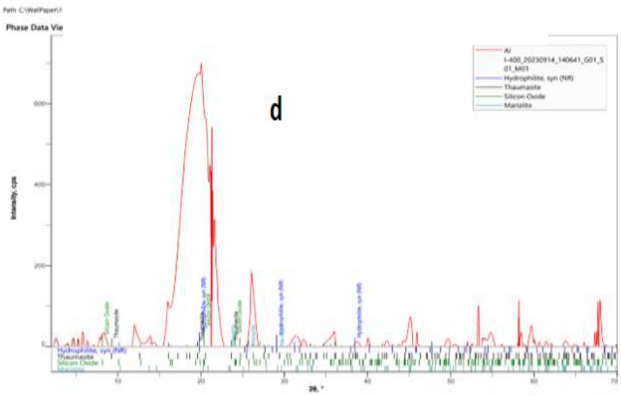

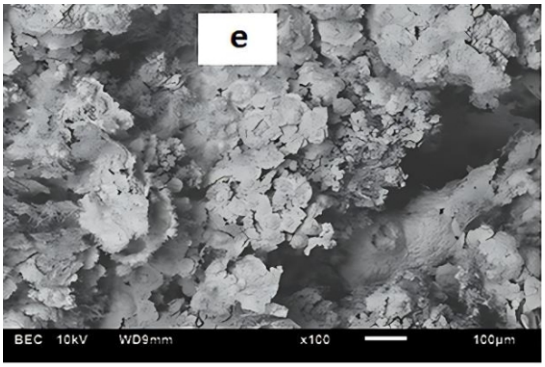

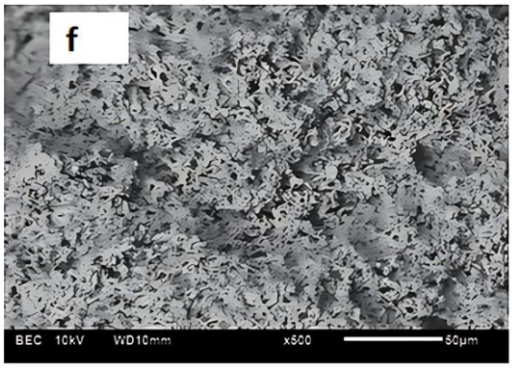

Figure 9 (a and b): FTIR spectra of HC and AHC respectively.
(c and d): XRD spectra of HC and AHC respectively.
(e and d): SEM morphology of HC and AHC respectively.

3.8 Mechanism of the Adsorption of Co^{2+} on to AHC

The FTIR spectra of the use AHC shown in Figure 10 confirmed the presence of hydroxyl (O-H), carboxyl (-C=O) groups which were involved in the adsorption process. At the end of the adsorption process, the FTIR results showed that the peaks at 3647 had shifted to 3224, cm^{-1} and had decreased in intensity in the used AHC. There were also additional shifts observed at 2357 cm^{-1}, 1650 and 1400 cm^{-1} which may be due to the presence of --COO which was masked in the unused AHC, indicating that the functional groups were involved in the adsorption process through surface complexation and chelation (Gao et al., 2020). There was an increase in the intensities of the peaks of used AHC as compared to unused AHC. This could be likely due to the presence of higher concentration of complexes form by the heavy metal and functional groups.

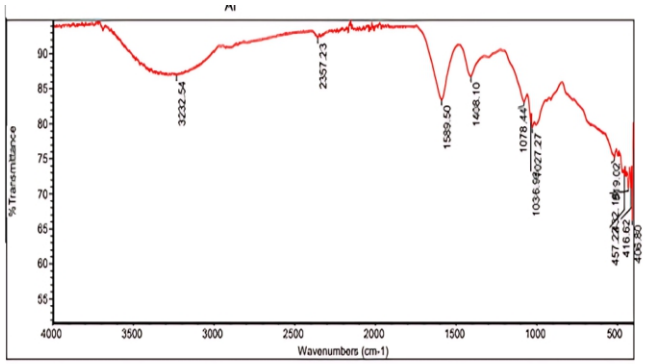

Figure 10: The FTIR spectra of spent AHC after the adsorption of Co^{2+}

The hydration of AHC resulted in the formation of CaO making the solution more alkaline through the formation of $Ca(OH)_2$ which later dissociated to OH^- according to Equation 14

$$CaO + H_2O \rightarrow Ca(OH)_2 \quad (14)$$

$$Ca(OH)_2 \Leftrightarrow Ca^{2+} + 2OH^-$$

$$(COO)^{2-}\ Ca^{2+} + Co^{2+} \rightarrow (COO)_2Co + Ca^{2+} \quad (15)$$

The Co^{2+} ion then forms carbonate and reacts with Co^{2+} by ion exchange as shown in Equation 15

4. Conclusion

The potential of kaolin-snail shell-plantain pseudo stem composite hydrochar and the alginate immobilized hydrochar to remove cobalt from waste water has been studied. The preliminary adsorption studies showed that AHC exhibited the highest removal efficiency (100%) as compared to the 94.56 and 91.04 of the pristine alginate beads and the hydrochar respectively. The enhanced adsorption efficiency of AHC was attributed to the synergistic effect between alginate and hydrochar, which provided abundant functional groups and improved structural properties. The Kinetic studies confirmed that the adsorption process followed a pseudo-second-order model, indicating that chemisorption played a dominant role. The results of the mass transfer studies suggest that intraparticle and film diffusion controlled the rate-limiting steps, with AHC exhibiting faster external mass transfer than HC. The equilibrium isotherm investigation established that the adsorption of Co^{2+} ions was best described by the Freundlich model for AHC at most temperatures, indicating multilayer adsorption on a heterogeneous surface, whereas the Langmuir model provided the best fit for HC at 35 °C, suggesting monolayer adsorption. The thermodynamic investigation confirmed that the adsorption process was spontaneous and exothermic, with high negative enthalpy values suggesting strong adsorbate-adsorbent interactions characteristic of chemisorption. The results suggest that AHC is a highly efficient and sustainable adsorbent for Co^{2+} ion removal, offering a promising alternative for heavy metal remediation in wastewater treatment applications. Future studies should focus on optimizing operational parameters, reusability and the application of the adsorbents to real wastewater treatment.

References

Agbale, N., Arinkoola, A., Ogunleye, O., & Agarry, S. (2023). Simultaneous Removal of Heavy Metals and Organics using Biosorbents: A Review. *Nigerian Research Journal of Engineering and Environmental Sciences, 8*(2), 403-418.

Agbale, N., Arinkoola, A., Ogunleye, O., & Agarry, S. (2024). Assessment of Engineered Snail Shell - Plantain Pseudo Stem Biochar Composite for the Remediation of Soils and Wastewater. *Nigerian Journal of Engineering, 31*(1), 2705-3954.

Ajibo, D. N., Orish, C. N., Ruggieri, F., Bocca, B., Battistini, B., Frazzoli, C., & Orisakwe, O. E. (2024). An update overview on mechanistic data and biomarker levels in cobalt and chromium-induced neurodegenerative disease. *Biological Trace Element Research, 202*(8), 538-3564.

Anastopoulos, I., & Kyzas, G. Z. (2016). Are the thermodynamic parameters correctly estimated in liquid-phase adsorption phenomenar. *Journal of Molecular Liquids, 218,* 174-185.

Awual, M. R., Ismael, M., & Yaita, T. (2014). Efficient detection and extraction of cobalt (II) from lithium ion batteries and wastewater by novel composite adsorbent. *Sensors and Actuators B: Chemical, 191,* 9-18.

Biswas, S., Sen, T., Yeneneh, A., & Charan, M. (2018). Synthesis and characterization of a novel Ca alginate-biochar composite as efficient zinc (Zn2+) adsorbent: Thermodynamics, process design,mass transfer and isotherm modeling. *Separation Science and Technology. doi:*DOI: 10.1080/01496395.2018.1527353

Boyd, G. E., Adamson, A. W., & Myers Jr, L. S. (1947). The exchange adsorption of ions from aqueous solutions by organic zeolites. II. Kinetics1. *Journal of the American Chemical Society, 69*(11), 2836-2848.

Chen, X. Q., Li, B., Shen, Y., & Guo, J. Z. (2019). Facile synthesis of calcite-impregnated hydrochar with high sorption capacity for Cu (II) from aqueous solution. *ACS omega, 4*(12), 15022-15029.

Chen, X., Li, B., Shen, Y., & Guo, J.-Z. (2019). Facile Synthesis of calcite-Impregnated hydrochar with high sorption capacity for Cu(II) from aqueoussSolution. *ACS Omega , 4,* 15022-15029.

de Araújo, T. P., Quesada, H. B., Dos Santos, D. F., da Silva Fonseca, B. C., Barbieri, J. Z., Bergamasco, R., & de Barros, M. A. (2022). Acetaminophen removal by calcium alginate/activated hydrochar composite beads: Batch and fixed-bed studies. Int. International *Journal of Biological Macromolecules, 203,* 553-562.

Egbosiuba, T. C., Tran, T. Q., Arole, K., Zhang, Y., Enyoh, C. E., & Mustapha, S. (2024). Results in Engineering. *Results in Engineering, 22, 102073., 22,* 102073.

Eva, V., Michal, G., Zuzana, D., Lukáš, K., & Christian, L. L. (2018). Production, characterization and adsorption studies of bamboo-based. *Waste Management 79* (2018) 385–394, 385-394.

Gao, L., Li, Z., Yi, W., Wang, L., Song, N., Zhang, W., & Zhang, A. (2023, 109074). Effective Pb2+ adsorption by calcium alginate/modified cotton stalk biochar aerogel spheres: With application in actual wastewater. *Journal of Environmental Chemical Engineering, 11*(1).

Gao, X., Guo, C., Hao, J., Zhao, Z., Long, H., & Li, M. (2020). Adsorption of heavy metal ions by sodium alginate based adsorbent-a review and new perspectivesomolecules, 164, 4423-4434. *International journal of biological macromolecule, 164,* 4423-4434. doi:https://doi.org /10.1016/j.ijbiomac.2020.09.046

González-Fernández, L. A., Medellín-Castillo, N. A., Navarro-Frómeta, A. E., Castillo-Ramos, V., Sánchez-Polo, M., & Carrasco-Marín, F. (2024). Optimization of hydrochar synthesis conditions for enhanced Cd (II) and Pb (II) adsorption in mono and multimetallic systems. *Environmental Research, 261,* 119651.

Gupta, B., Mishra, A., Singh, R., & Thakur, I. S. (2021). Fabrication of calcite based biocomposites for catalytic removal of heavy metals from electroplating industrial effluent. *Environmental Technology & Innovation, 21,* 101278.

Gürkan, E. H., & İlyas, B. (2022). Adsorption of copper, and zinc onto novel Ca-lginate-biochar composite prepared by biochars produced from pyrolysis of groundnut hus. *International Journal of Phytoremediation, 24*(13), 1350-1363.

Incan, N., Hawboldt, K. A., & MacQuarrie, S. (2024). Hydrothermal carbonization of snow crab processing by-product: Hydrochar characterization. Journal of Analytical and Applied Pyrolysis, 183, 106767. *Journal of Analytical and Applied Pyrolysis, 183.*

Islam, M. A., Morton, D. W., Johnson, B. B., Pramanik, B. K., Mainali, B., & Angove, M. J. (2018). Opportunities and constraints of using the innovative adsorbents for the removal of cobalt (II) from wastewater: A review. *Environmental Nanotechnology, Monitoring & Management, 10, 435-456., 10,* 435-456.

Joel, L., Umaru Jongur, A., Adebayo, E., & Michael, A. (2022). Economics of plantain production among farmers in Northeast Nigeria. Turkish *Journal of Agriculture -Food Science and Technology, 10*(4), 536-541. doi:DOI:https://doi.org/10.24925/turjaf.v10i4.536-541.450

Kushwaha, R., Singh, R. S., & Mohan, D. (2024). Enhanced arsenic removal using biochar immobilized bacteria encapsulated in polyvinyl alcohol-sodium alginate beads: Fabrication, optimization and performance evaluation. *Journal of Water Process Engineering, 64,* 105509.

Lagergren, S. (1898). Zur Theorie der sogenannten Adsorption gelöster Stoffe. K Sven Vetenskapsakad. *Handl, 24,* 1–3. doi:doi:10.1371/journal.pone.0167428

Lim, Y., Kim, B., Jang, J., & Lee, D. S. (2022). Buckwheat hull-derived biochar immobilized in alginate beads for the adsorptive removal of cobalt from aqueous solutions. . *Journal of Hazardous Materials, 436,* 129245.

Navarro, A., Musaev, H., Serrano, K., & Masud, M. (2014). Adsorption kinetics of cobalt (II) Ions onto alginate beads from aqueous solutions. *J Earth Science Climate Change, 5*(23).

Nguyen, L. H., Van, H. T., Chu, T. H., Nguyen, T. H., & Nguyen, T. D. (2020). Paper waste sludge-derived hydrochar modified by iron (III) chloride for enhancement of ammonium adsorption: An adsorption mechanism study. *Technology & Innovation, 21.*

Nimbalkar, M. N., & Bhat, B. R. (2021). Simultaneous adsorption of methylene blue and heavy metals from water using Zr-MOF having free carboxylic group. *Journal of Environmental Chemical Engineering, 9*(5), 106216. doi:https://doi.org/10.1016/j.jece.2021.106216

Panic, S., Guzsvány, V., Kónya, Z., Kukovecz, Á., & Boskovic, G. (2017). Kinetic, equilibrium and thermodynamic studies of thiamethoxam adsorption by multi-walled carbon nanotubes. *International Journal of Environmental Science and Technology, 14,* 1297-1306.

Rachdi, Y., El Alouani, M., Bassam, R. M., Saufi, H., El Khattabi, E. H., & Belaaouad, S. (2023). Treatment of water contaminated by cadmium using low-cost and eco-friendly alginate/Moroccan clay composite. *Desalination and Water Treatment, 298,* 81-92.

Rafiq, M. K., Joseph, S. D., Li, F., Bai, Y., Shang, Z., Rawal, A., & Long, R. J. (2017). Pyrolysis of attapulgite clay blended with yak dung enhances pasture growth and soil health: Characterization and initial field trials. *Science of the Total Environment, 607,* 184-194. doi:https://doi.org/10.1016/j.scitotenv.2017.06.186

Rasheed, F. A., Sillanpää, M., & Moradi, M. (2024). Cobalt adsorption by Ca (OH) 2 Modified quartz rock particles adsorbent: Equilibrium isotherm, kinetics, and thermodynamic studies. *Desalination and Water Treatment, 319,* 100477.

Reddy, D. H., & Lee, S. M. (2014). Magnetic biochar composite: facile synthesis, characterization, and application for heavy metal removal. *Colloids and Surfaces A: Physicochemical and Engineering Aspects, 45,* 96-103. doi:https://doi.org/10.1016/j.colsurfa.2014.03.105

Reichenberg, D. (1953). Properties of ion-exchange resins in relation to their structure. III.Kinetics of exchange. *J. Am. Chem. Soc, 75,* 589–597.

Sharma, A., Sharma, G., Naushad, M. G., & Pathania, D. (2018). Remediation of anionic dye from aqueous system using bio-adsorbent prepared by microwave activation. *Environmental technology, 39*(7), 917-930.

Shin, J., Kwak, J., Lee, Y., Kim, S., Choi, M., Bae, S., . . . Chon, K. (2020). Competitive adsorption of pharmaceuticals in lake water and wastewater effluent by pristine and NaOH-activated biochars from

spent coffee wastes: Contribution of hydrophobic and p-p interactions . *Environmental Pollution* , 116244.

Singh, A. (2016). Chapter 8 - Nanoparticle Ecotoxicology,. In A. Singh, *Engineered Nanoparticles,* (pp. 243-450). Academic Press.

Thakur, S., Sharma, B., Verma, A., Chaudhary, Y., & Thakur, V. (2018). Recent Progress in Sodium Alginate Based Sustainable Hydrogels for Environmental Applications. *Journal of Cleaner Environment, 198,* 143-159.

Touihri, M., Guesmi, F., Hannachi, C., Hamrouni, B., Sellaoui, L., Badawi, M., . . . Fiol, N. (2021). Single and simultaneous adsorption of Cr(VI) and Cu (II) on a novel Fe3O4/pine cones gel beads nanocomposite: Experiments, characterization and isotherm modelling. *Chemical Engineering Journal,* 416 .

Wan, T., Tang, Q., Wang, T., Wang, J., Jia, Y., & Yu, M. (2022). Adsorption behaviours of copper (II), lead (II), and cadmium (II) ions from aqueous solution by polyethylenimine-modified magnetic hydrogel nanocomposites. *Journal of Polymer Research, 29*(12), 520.

Wang, B., Gao, B., Zimmerman, A. R., Zheng, Y., & Lyu, H. (2018). Novel biochar-impregnated calcium alginate beads with improved water holding and nutrient retention properties. *Journal of environmental management,, 209,* 105-111.

Wang, J., & Guo, X. (2020). Adsorption kinetic models: Physical meanings, applications, and solving methods. *Journal of Hazardous Materials,* 390.

Wang, S., Zhong, S., Zheng, X., Xiao, D., Zheng, L., Yang, Y., & Sheng, Z. (2021). Calcite modification of agricultural waste biochar highly improves the adsorption of Cu (II) from aqueous solutions. *Journal of Environmental Chemical Engineering, 9*(5).

Xu, X., Zhao, Y., Sima, J., Zhao, L., Mašek, O., & Cao, X. (2017). Indispensable role of biochar-inherent mineral constituents in its environmental applications: A review. *Bioresource Technology, 241,* 887-899.

Yakub, E., Agarry, S. E., Omoruwou, F., & Owabor, C. N. (2020). Comparative study of the batch adsorption kinetics and mass transfer in phenol-sand and phenol-clay adsorption systems. *Particulate Science and Technology.,* 801-811. doi: https://doi.org/10.1080/02726351.2019.1616862

Yakub, E., Agarry, S., Omoruwou, F., & Owabor, C. (2019). Comparative study of the batch adsorption kinetics and mass transfer in phenol-sand and phenol-clay adsorption systems. *Particulate Science and Technology,.* doi:https://doi.org/10.1080/02726351.2019.1616862

Yoon, K., Cho, D. W., Tsang, D. C., Bolan, N., Rinklebe, J., & Song, H. (2017). Fabrication of engineered biochar from paper mill sludge and its application into removal of arsenic and cadmium in acidic water. *Bioresource technology, 246,* 69-75.

Younis, A., Motawe, E., Moustafa, Y., & Kim, K. (2020). A strategy for the efficient removal of chlorophenols in petrochemical wastewater by organophilic and aminated silica@alginate microbeads:Taguchi optimazation and isotherm modeling based on partition coefficient. *Journal of Hazardous Material, 397,* 122792.

Yu, J., Feng, H., Tang, L., Pang, Y., Wang, J., Zou, J., & Wang, J. (2021). Insight into the key factors in fast adsorption of organic pollutants by hierarchical porous biochar. *Journal of hazardous materials, 403,* 123610. doi:https://doi.org/10.1016/j.jhazmat.2020.123610

Zaghouane-Boudiaf, H., Boutahala, M., Sahnoun, S., Tiar, C., & Gomri, F. (2014). Adsorption characteristics, isotherm, kinetics, and diffusion of modified natural bentonite for removing the 2, 4, 5-trichlorophenol. *Applied clay science,* 81-87. doi:https://doi.org/10.1016/j.clay.2013.12.030

Zamora-Ledezma, C., Negrete-Bolagay, D., Figueroa, F., Zamora-Ledezma, E., Ni, M., Alexis, F., & Guerrero, V. (2021). Heavy metal water pollution: A fresh look about hazards, novel and conventional remediation methods. *Environmental Technology & Innovarion,* 22.

Zhao, R., Ding, W., Sun, M., Yang, L., Liu, B., Zheng, H., & Li, H. (2022). Insight into the co-removal of Cu (II) and ciprofloxacin by calcite-biochar composite: Enhancement and competition. *Separation and Purification Technology, 287,* 120487.

Zhao, X., Zheng, M., Gao, X., Zhang, J., Wang, E., & Gao, Z. (2021). The application of MOFs-based materials for antibacterials adsorption. *Coordination Chemistry Reviews,* 213970. doi:https://doi.org/10.1016/j.ccr.2021.213970